Layer-locked anomalous valley Hall effect in a two-dimensional *A*-type tetragonal antiferromagnetic insulator

San-Dong Guo,[1,*,†] Wei Xu,[2,†] Yang Xue,[3] Gangqiang Zhu,[4] and Yee Sin Ang[5,‡]

[1]*School of Electronic Engineering, Xi'an University of Posts and Telecommunications, Xi'an 710121, China*
[2]*State Key Laboratory of Surface Physics and Key Laboratory of Computational Physical Sciences (MOE), and Department of Physics, Fudan University, Shanghai 200433, China*
[3]*Department of Physics, East China University of Science and Technology, Shanghai 200237, China*
[4]*School of Physics and Electronic Information, Shaanxi Normal University, Xi'an 716000, Shaanxi, China*
[5]*Science, Mathematics and Technology (SMT) Cluster, Singapore University of Technology and Design, Singapore 487372*

(Received 21 November 2023; accepted 2 April 2024; published 17 April 2024)

Antiferromagnetic (AFM) spintronics provides a route towards energy-efficient and ultrafast device applications. Achieving anomalous valley Hall effect (AVHE) in AFM monolayers is thus of considerable interest for both fundamental condensed-matter physics and device engineering. Here we propose a route to achieve an AVHE in A-type AFM insulator composed of vertically stacked monolayer quantum anomalous Hall insulators with strain and electric field modulations. Uniaxial strain and electric field generate valley polarization and spin splitting, respectively. Using first-principles calculations, Fe_2BrMgP monolayer is predicted to be a prototype hosting *valley-polarized quantum spin Hall insulators* in which AVHE and quantum spin Hall effect are synergized in a single system. Our findings reveal a route to achieve multiple Hall effects in two-dimensional tetragonal AFM monolayers.

DOI: 10.1103/PhysRevB.109.134426

I. INTRODUCTION

Utilizing valley degree of freedom to encode and process information, characterized as valleytronics, provides remarkable opportunities for developing next-generation minimized devices [1–7]. Valley refers to a local energy minimum/maximum in conduction/valence bands, where these energy extremes are robust against phonon and impurity scattering due to the large separation in the momentum space [1]. Recent proposals of valleytronics are mainly based on time-reversal-connected valleys, where valley polarization is induced by an external field, dynamically or electrostatically [8–13]. Intrinsic valleytronics materials with spontaneous valley polarization are more advantageous in terms of valley robustness, energy efficiency, and simplicity in operation, which are beneficial for practical device applications. Recently, the ferrovalley (FV) semiconductor has been proposed [14], which possesses spontaneous valley polarization induced by the combined effects of magnetic order and spin-orbit coupling (SOC). Valley-dependent Berry curvature in FV materials leads to the anomalous valley Hall effect (AVHE). FV materials thus offer an interesting platform to study valley-contrasting transport and Berry physics.

Achieving spontaneous valley polarization typically requires a ferromagnetic (FM) system as a basic premise [15]. Compared with ferromagnetism, antiferromagnetic (AFM) materials with zero magnetic moment are inherently robust to external magnetic perturbation and possess ultrafast dynamics [16,17], thus offering enormous potential for both valleytronic and spintronic applications. However, spontaneous valley polarization in AFM materials is rarely reported [18–22], and the AVHE in AFM systems is undesirably suppressed [19,20]. Furthermore, topological states based on the valley-polarized quantum anomalous Hall insulator (VQAHI) have been recently proposed, in which valley polarization and the quantum anomalous Hall effect (QAHE) are combined in one material. Such a system is particularly interesting due to its compatibility with low-power electronics, spintronics, sensing, metrology, and quantum information processing applications [23–25]. Several VQAHI systems have been theoretically proposed by constructing complex heterostructure, layer-dependent proximity effects, and accurate regulation of strain and correlation strength [26–40]. It is worth noting that the quantum anomalous Hall state of the "valley-polarized quantum anomalous Hall state" in twisted graphene and transition-metal dichalcogenides occurs exactly because of the valley polarization, and the electron interactions spontaneously polarize the valleys at special fillings in these twisted systems [41–43]. The "valley-polarized quantum anomalous/spin Hall state" referred to in our work means that the valley polarization and quantum anomalous/spin Hall state can coexist, and the valley polarization is not the direct cause of the quantum anomalous/spin Hall state.

It should also be noted that previously reported valley-polarized AFM systems are mostly based on hexagonal symmetric lattice [18–22]. Whether FV can be achieved in

*sandongyuwang@163.com
†These authors contributed equally to this work.
‡yeesin_ang@sutd.edu.sg

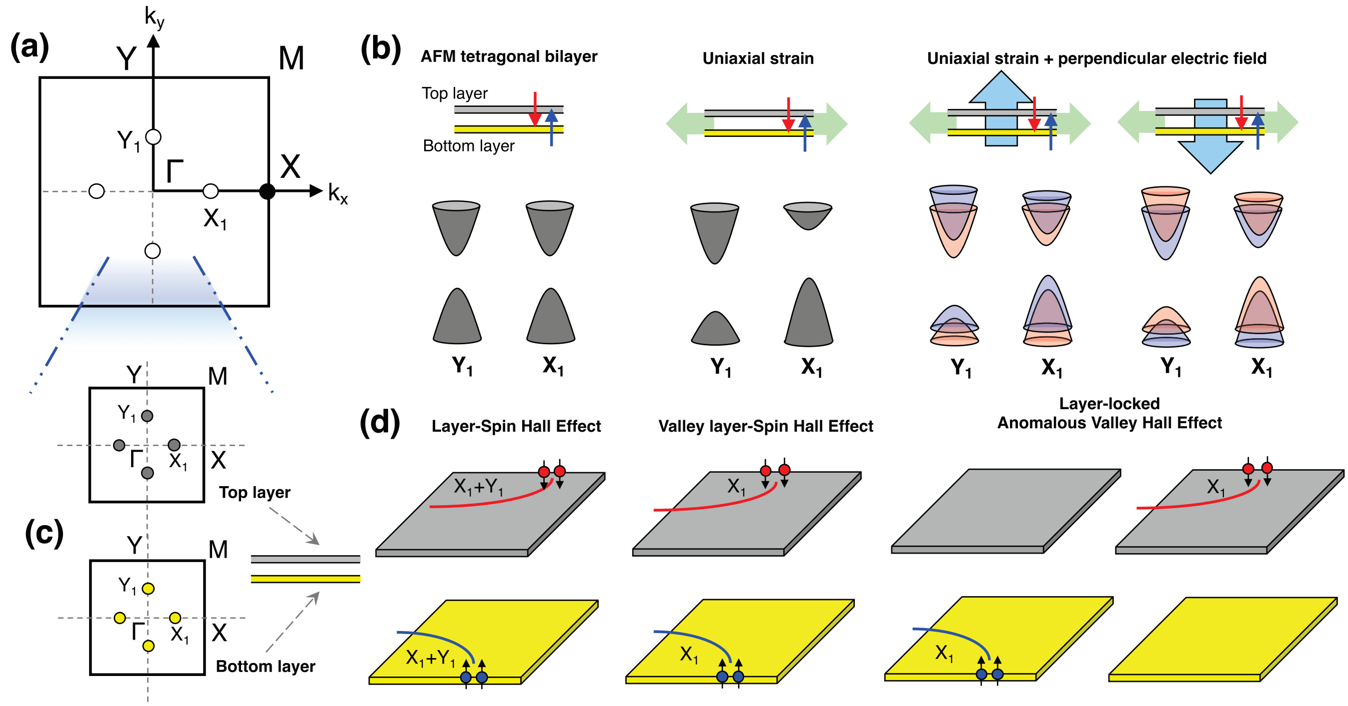

FIG. 1. Concept of layer-locked anomalous valley Hall effect in 2D tetragonal lattice. (a) 2D tetragonal lattice possesses equivalent valleys along Γ-X and Γ-Y lines with Berry curvature mainly occurring around Y_1 and X_1 valleys. (b) Applying uniaxial strain along the x direction makes the Y_1 and X_1 valleys become unequal but spin degeneracy is still preserved. Simultaneous application of uniaxial strain and the out-of-plane electric field further breaks the spin degeneracy. Reversing the electric field leads to opposite spin splitting at both Y_1 and X_1 valleys. The spin-up and spin-down channels are depicted in blue and red, respectively. (c) Superposition of two tetragonal QAHIs with equal but opposite magnetic moments (A-type AFM order) leads to spin-degenerate equivalent Y_1 and X_1 valleys with net-zero Berry curvature in momentum space. However, the Berry curvatures for the spin-up and spin-down channels are positive and negative, respectively, yielding nonzero layer-locked hidden Berry curvature in real space. (d) The layer–spin Hall effect, the valley layer–spin Hall effect, and the layer-locked anomalous valley Hall effect.

AFM system beyond hexagonal lattice symmetry remains an open question thus far. Can AVHE in AFM materials be achieved in a system beyond hexagonal lattices? Is it possible to achieve other valley-polarized topological states? Here we propose a way to realize AVHE in an A-type tetragonal AFM insulator composed of vertically-stacked monolayered quantum anomalous Hall insulators (QAHI) under both strain and electric field tuning. A peculiar valley-polarized quantum spin Hall insulator (VQSHI) can be achieved in the proposed systems, which is verified via first principles in Fe_2BrMgP monolayer as a prototype VQSHI. Our findings open up a previously unexplored concept of VQSHI in which valley polarization and the quantum spin Hall effect (QSHE) are synergized in a single system.

II. ACHIEVING AVHE IN AFM INSULATORS

Firstly, a two-dimensional (2D) tetragonal FM QAHI is used as the basic building block, which has a layer of magnetic atoms and possesses equivalent valleys along the Γ-X and Γ-Y lines in the first Brillouin zone (BZ) due to C_4 rotation symmetry [Fig. 1(a)]. The Berry curvatures mainly occur around the Y_1 and X_1 valleys with positive values.

To realize the AFM insulator, a superposition of two 2D tetragonal FM QAHIs with equal but opposite magnetic moments (A-type AFM order) is constructed [Fig. 1(b)], giving rise to spin degeneracy and equivalent Y_1 and X_1 valleys. Here, we assume that the AFM system has a symmetry of a combination of inversion symmetry $\mathcal{P}$ and time-reversal symmetry $\mathcal{T}$ ($\mathcal{PT}$), which leads to a spin-degenerate 2D system. To induce valley polarization, a natural way is to destroy C_4 rotation symmetry via uniaxial strain along the x or y direction [Fig. 1(b)]. However, the spin degeneracy is still maintained under uniaxial strain, which prohibits the AVHE. An out-of-plane electric field $E_\perp$ is introduced to break the $\mathcal{PT}$ symmetry, which lifts the spin degeneracy of valleys [Fig. 1(b)]. Such spin-degeneracy breaking is due to the layer-dependent electrostatic potential $\propto eEd$ (e and d denote the electron charge and the layer distance) created by the out-of-plane electric field, which causes the spin-up and spin-down bands in different layers to stagger, leading to the spin-splitting effect. A similar mechanism can be found in electric potential difference antiferromagnetism [44]. More interestingly, the spin orders at both Y_1 and X_1 valleys can be reversed through reversing the direction of out-of-plane electric field [Fig. 1(b)], thus offering electrostatic-field-tunable valley polarization.

The superposition of two tetragonal QAHIs leads to zero Berry curvature $\Omega(k)$ in momentum space due to $\mathcal{PT}$ symmetry [Fig. 1(c)]. However, each layer breaks the $\mathcal{PT}$ symmetry *individually*, which gives rise to the layer-locked *hidden* Berry curvature, and the Berry curvatures for the spin-up and spin-down channels are positive and negative-valued, respectively. Such layer-locked hidden Berry curvature leads to a peculiar layer-Hall effect not commonly found in other AVHE systems.

In the presence of a longitudinal in-plane electric field $E_{\parallel}$, the Bloch carriers acquire an anomalous transverse velocity $v_{\perp} \sim E_{\parallel} \times \Omega(k)$ [4]. By shifting the Fermi level in the valence band via hole doping, various layer–spin Hall and layer-locked AVHE can occur [Fig. 1(d)]:

(i) The spin-up and spin-down electrons from Y_1 and X_1 valleys accumulate along opposite sides of different layers in the case of the 2D A-type tetragonal AFM system, resulting in the layer–spin Hall effect.

(ii) When a uniaxial strain is applied, the spin-up and spin-down electrons from only the X_1 valley accumulate along the opposite sides of different layers, resulting in the valley layer–spin Hall effect.

(iii) The spin-up/spin-down electrons from only X_1 valley accumulate along one side of bottom/top layer, resulting in the rarely explored *layer-locked anomalous valley Hall effect*.

III. MATERIAL REALIZATION

Monolayer Fe_2XY ($X =$ or $\neq Y =$ Cl, Br, and I) and Li_2Fe_2XY ($X =$ or $\neq Y =$ S, Se, and Te) families [45–50] can be used as the basic building blocks. These monolayers are tetragonal QAHIs with equivalent valleys along the Γ-X and Γ-Y lines in the first Brillouin zone (BZ), and the extremes of Berry curvatures are located at the Y_1 and X_1 valleys. Instead of employing the vertical stacking of two identical monolayers via the van der Waals heterostructure approach, we consider an intercalation architecture in which two identical monolayers are intercalated to form an "ultra-thick" Fe_2XYP monolayer ($X =$ Br, Cl, and I; $Y =$ Mg and Be) [51]. We use Fe_2BrMgP as a protype system to illustrate the concept of the layer-locked AVHE in a 2D tetragonal AFM system.

IV. COMPUTATIONAL DETAIL

The spin-polarized first-principles calculations are performed within density functional theory [52], as implemented in VASP code [53–55] within the projector augmented-wave method. We adopt the generalized gradient approximation of Perdew-Burke-Ernzerhof [56] as the exchange-correlation functional. The kinetic energy cutoff of 500 eV, the total energy convergence criterion of 10^{-8} eV, and the force convergence criterion of 0.001 eV Å^{-1} are set to obtain the accurate results. To account for the localized nature of 3d orbitals of Fe atoms, a Hubbard correction $U_{\text{eff}} = 2.5$ eV [51] is employed within the rotationally invariant approach proposed by Dudarev *et al.* [57], and the SOC is incorporated for investigation of electronic structures. To avoid adjacent interactions, the vacuum space along the z direction is set to more than 16 Å. A $12 \times 12 \times 1$ Monkhorst-Pack k-point mesh is used to sample the BZ for calculating electronic structures and elastic properties.

The elastic stiffness tensors C_{ij} are calculated by using the strain-stress relationship (SSR) method. The 2D elastic coefficients C_{ij}^{2D} have been renormalized by $C_{ij}^{\text{2D}} = L_z C_{ij}^{\text{3D}}$, where L_z is the length of the unit cell along the z direction. The topological properties are studied with the maximal localized Wannier function tight-binding model by WANNIER90 and WANNIERTOOLS [58,59].

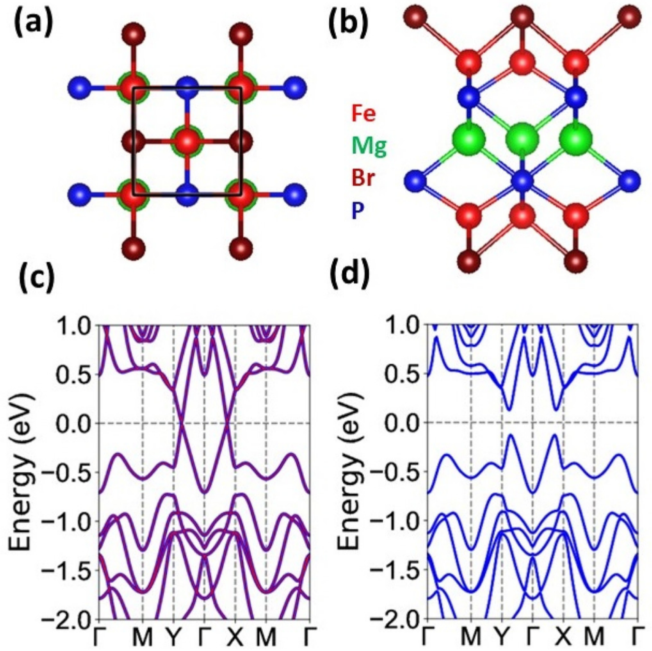

FIG. 2. Lattice and electronic structures of Fe_2BrMgP monolayer. (a) and (b) Top and side views of monolayer Fe_2BrMgP. Energy band structures of Fe_2BrMgP monolayer (c) without and (d) with SOC. In panel (c), the spin-up and spin-down channels are depicted in blue and red.

V. LATTICE, MAGNETIC, AND ELECTRONIC PROPERTIES

Fe_2BrMgP monolayer is dynamically, mechanically, and thermally stable [51]. The crystal structures of Fe_2BrMgP monolayer are plotted in Figs. 2(a) and 2(b), crystallizing in the $P4/nmm$ space group (No. 129). The unit cell contains ten atoms with a seven-atom layer sequence of Br-Fe-P-Mg-P-Fe-Br. The optimized equilibrium lattice constants are $a = b = 4.03$ Å by GGA + U method. To determine the ground state of Fe_2BrMgP, we consider four magnetic configurations, including FM ordering, AFM1 ordering (A-type AFM ordering), AFM2 ordering, and AFM3 ordering (see Fig. S1 [60]). This A-type AFM ordering is predicted to be the ground state, and its energy is 55/645/759 meV per unit cell lower than that with the FM/AFM2/AFM3 ordering. The Fe_2BrMgP monolayer is centrosymmetric. However, when spin is considered, the inversion symmetry $\mathcal{P}$ is missing for A-type AFM ordering, and the time-reversal symmetry $\mathcal{T}$ is also lacking. A combination of inversion symmetry $\mathcal{P}$ and time-reversal symmetry $\mathcal{T}$ gives this $\mathcal{PT}$ preserving: the $\mathcal{T}$ operation reverses the spin direction of each Fe atom, followed by the $\mathcal{P}$ operation which swaps the top and bottom Fe atoms. The different magnetic orientation can affect the symmetry of a system as well as the valley and topological properties [34–40,45–50]. For example, in monolayer Fe_2Br_2,

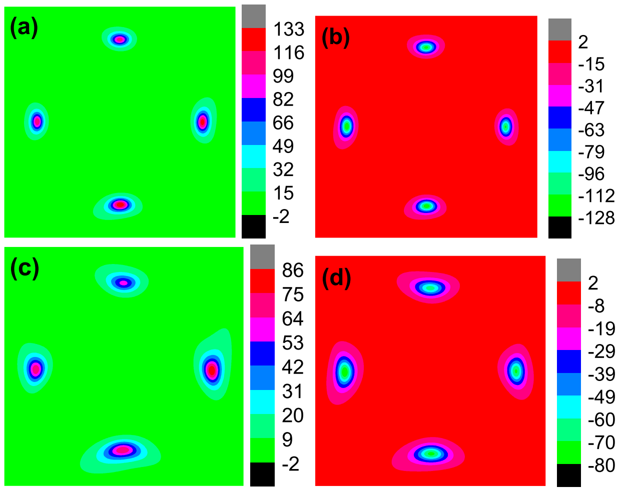

FIG. 3. Layer-dependent Berry curvature of Fe_2BrMgP. The Berry curvatures are shown for the spin-up (a, c) and spin-down (b, d) channels for $a/a_0 = 1.00$ and $E = 0.00$ V/Å (a, b) and for $a/a_0 = 1.04$ and $E = 0.02$ V/Å (c, d).

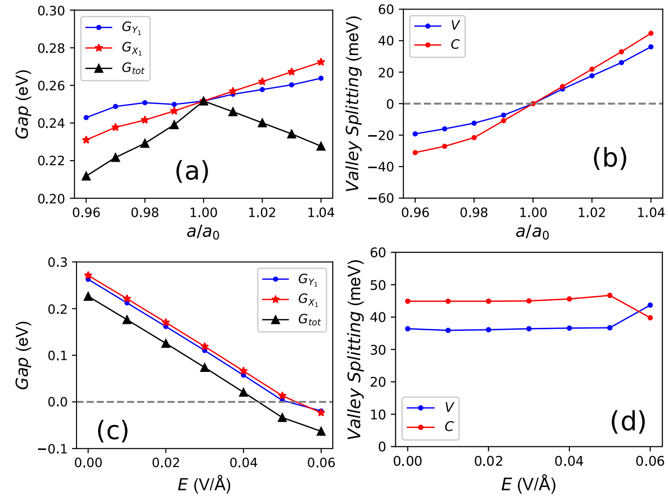

FIG. 4. Strain and electric field modulation. For Fe_2BrMgP, the related band gaps including the global gap (G_{tot}) and gaps of Y_1 and X_1 valleys (G_{Y_1} and G_{X_1}) (a, c), and valley splitting for both valence (V) and condition (C) bands (b, d) as a function of a/a_0 (a, b) and E (c, d) with $a/a_0 = 1.04$.

when the magnetic orientation is out-of-plane, the hot spots in the Berry curvature are around four gapped Dirac cone with the same signs, leading to Chern number $C = 2$; while for in-plane magnetization, two of four main hot spots in the Berry curvature have the opposite sign of the other two, giving rise to a vanishing Chern number [49]. For our proposed system, an out-of-plane magnetic orientation is needed, and the magnetic orientation can be determined by the magnetic anisotropy energy (MAE). By the GGA + U + SOC method, the MAE can be calculated as $E_{\text{MAE}} = E_{SOC}^{||} - E_{SOC}^{\perp}$, where || and ⊥ denote the in-plane spin orientation and the out-of-plane spin orientation, respectively. The MAE is 451 μeV/Fe, and the positive value indicates the out-of-plane easy magnetization axis of Fe_2BrMgP, which confirms our proposed design principles. The total magnetic moment per unit cell is strictly 0.00 μ_B, and the magnetic moments of bottom and top Fe atoms are 3.06 and −3.06 μ_B, respectively.

The calculated energy band structures of Fe_2BrMgP without and with SOC are shown in Figs. 2(c) and 2(d), respectively. When neglecting SOC, two pairs of band-crossing points occur near the Fermi level along the Γ-X and Γ-Y lines. With SOC, a Dirac gap of 252 meV is introduced, yielding equivalent valleys along the Γ-X and Γ-Y lines due to the C_4 rotation symmetry. The corresponding k points in the momentum space are marked by X_1 and Y_1 without valley splitting ($\Delta E_C = E_{X_1}^C - E_{Y_1}^C$ and $\Delta E_V = E_{X_1}^V - E_{Y_1}^V$) for both conduction and valence bands. Because of the $\mathcal{PT}$ symmetry, the bands of Fe_2BrMgP are spin degenerate both without and with SOC.

Because of the $\mathcal{PT}$ symmetry, the Berry curvature of Fe_2BrMgP vanishes. However, each layer breaks the $\mathcal{PT}$ symmetry locally, and such layer-specific symmetric breaking leads to a nonvanishing layer-locked hidden Berry curvature. Here the Berry curvatures of spin-up and spin-down channels are nonzero [Figs. 3(a) and 3(b)]. The Berry curvatures are opposite for spin-up and spin-down channels around the Y_1 and X_1 valleys, respectively. In the presence of a longitudinal in-plane electric field $E_{\parallel}$, the spin-up and spin-down electrons from the Y_1 and X_1 valleys accumulate along opposite sides of the top and bottom Fe layers, resulting in the layer–spin Hall effect [Fig. 1(d)].

VI. UNIAXIAL STRAIN INDUCES VALLEY POLARIZATION

To induce valley polarization in Fe_2BrMgP, a uniaxial strain along the x or y direction is applied which reduces C_4 to C_2 symmetry. The valleys along the Γ-X and Γ-Y lines become inequivalent, thus giving rise to valley polarization. We use a/a_0 (0.96 to 1.04) to simulate a uniaxial strain along the x direction, and the lattice constant b along the y direction is optimized. The in-plane Young's modulus $C_{2\text{D}}(\theta)$ as a function of the angle θ relative to the x direction is plotted in Fig. S2 [60]. The obtained $C_{2\text{D}}$ along the x direction is 86 Nm^{-1}. This is smaller than those of graphene (∼340 ± 40 Nm^{-1}) and MoS_2 (∼126.2 Nm^{-1}) [61,62], which indicates the better mechanical flexibility of Fe_2BrMgP, thus favoring the experimental realization of valley polarization by strain. The strained Fe_2BrMgP remains in the A-type AFM ground state with out-of-plane magnetic anisotropy within the considered strain range (see Fig. S3 [60]).

The electronic band structures of strained Fe_2BrMgP calculated using GGA + SOC are plotted in Fig. S4 [60]. The evolutions of the band gap and the valley splitting (ΔE_V and ΔE_C) for both valence and conduction bands as a function of a/a_0 are plotted in Figs. 4(a) and 4(b). The uniaxial strain induces valley polarization for both conduction and valence bands, and the valley polarization can be switched between X_1 and Y_1 valleys with strain transiting from compressive to tensile cases. For common hexagonal FV systems, the valley polarization can be reversed by the magnetic field [34–39]. Therefore, the uniaxial strain can be regarded as a pseudomagnetic field for the tetragonal system [40]. For $a/a_0 = 0.96/1.04$, the corresponding valley splitting is

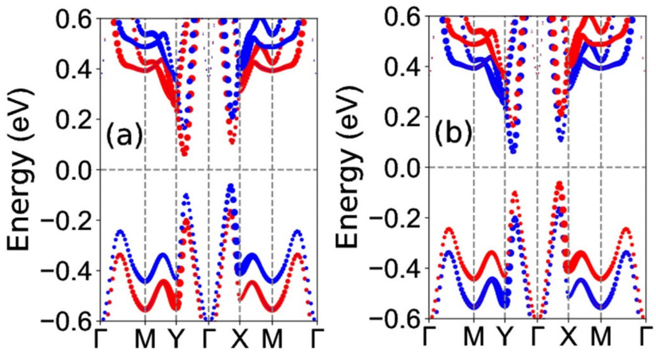

FIG. 5. Sign-reversible layer-locked anomalous valley Hall effect. For Fe_2BrMgP with $a/a_0 = 1.04$, the spin-resolved energy band structures for $E = +0.02$ V/Å (a) and $E = -0.02$ V/Å (b) are shown. The spin-up and spin-down channels are depicted in blue and red.

-19 (-31) meV/36 (45) meV for the valence (conduction) band, which is close to or larger than the thermal energy of room temperature (25 meV). Using $a/a_0 = 1.04$ as a representative, the Berry curvatures of the spin-up and spin-down channels are plotted in Fig. S5 [60]. The Berry curvatures are opposite for spin-up and spin-down channels around Y_1 and X_1 valleys. In this case, a longitudinal in-plane electric field $E_\parallel$ can thus lead to the accumulation of the spin-up and spin-down electrons from only X_1 valleys along the opposite sides of the top and bottom Fe layers, resulting in the valley layer–spin Hall effect as illustrated in Fig. 1(d).

VII. ELECTRIC FIELD INDUCES SPIN SPLITTING

An out-of-plane electric field can break the $\mathcal{PT}$ symmetry to lift the spin degeneracy of the valleys. Taking strained Fe_2BrMgP with $a/a_0 = 1.04$ as an example, the electric field (E) effects on the electronic structures are investigated. The difference between $+E$ and $-E$ is that the spin-splitting order is reversed. According to Fig. S6 [60], the ground state of Fe_2BrMgP remains in the A-type AFM ordering with out-of-plane magnetic anisotropy within the considered E range. The energy band structures of Fe_2BrMgP by using GGA + SOC at representative E are plotted in Fig. S7 [60], and the spin-resolved energy band structures at $E = \pm 0.02$ V/Å are shown in Fig. 5. The evolutions of related energy band gap and the valley splitting for both valence and condition bands as a function of E are plotted in Figs. 4(c) and 4(d). In fact, by constructing the Janus structure $Fe_4BrIMg_2P_2$, the external electric field can be equivalently replaced by the build-in electric field to achieve spin splitting (see Fig. S8 [60]).

The spin splitting induced by the out-of-plane electric field, and spin-polarization reversal via reversing the direction of electric field, can be observed in Fig. 5. The electric field can maintain the valley splitting amplitude and induce a semiconductor-metal phase transition [see Figs. 4(c) and 4(d)]. The sizes of spin splitting at X_1 and Y_1 valleys for both conduction and valence bands are plotted in Fig. S9 [60], which meets the layer-dependent electrostatic potential $\propto eEd$ (The sizes of spin splitting can be calculated by eEd). Using $E = 0.02$ V/Å as an example, the Berry curvature calculations in Figs. 3(c) and 3(d) show that the Berry curvatures of spin-up and spin-down channels around Y_1 and X_1 valleys are opposite. In the presence of a longitudinal in-plane electric field $E_\parallel$, the spin-up electrons from only the X_1 valley accumulate along one side of the bottom Fe layer, which leads to the layer-locked anomalous valley Hall effect of Fig. 1(d). When the direction of the electric field is reversed, the spin-down electrons from only the X_1 valley accumulate along the other side of the top Fe layer, leading to a electric-field-effect-induced sign reversal of the AVHE previously predicted in the FV-FM system [63].

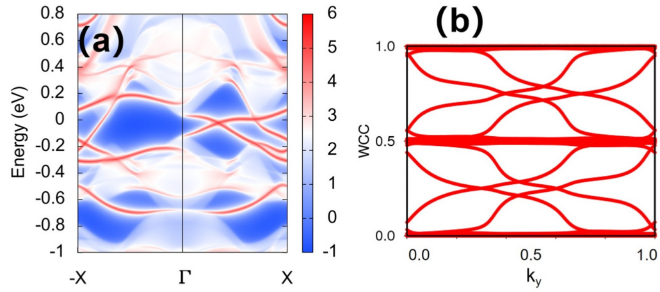

FIG. 6. Topological properties of Fe_2BrMgP. For Fe_2BrMgP with $a/a_0 = 1.04$ at $E = +0.02$ V/Å: (a) the edge states along the [100] direction; (b) the evolution of WCCs along k_y.

VIII. VALLEY-POLARIZED QUANTUM SPIN HALL INSULATOR

In a 2D AFM insulator, one cannot define a $Z2$ invariant, which can be defined in a $\mathcal{T}$-preserved quantum spin Hall insulator (QSHI). To realize an AFM QSHI, a way is to create a z-component spin (s_z) conserved superposition of two quantum anomalous Hall insulators with equal but opposite magnetic moments [64]. If the constructed AFM systems have a symmetry of a combination of $\mathcal{P}$ and $\mathcal{T}$ ($\mathcal{PT}$), the states with different s_z in one branch are orthogonal to each other and belong to different irreducible representations, and then the spin Chern number C_s can still be well-defined [51].

To follow this proposal, the Fe_2BrMgP has been predicted to be an AFM QSHI with high spin Chern numbers, as confirmed by the gapless edge states and the topological invariant spin Chern numbers C_s [51]. By applying uniaxial strain and the electric field simultaneously, the VQSHI can be achieved in Fe_2BrMgP, which combines AVHE and QSHE in one material, providing a path towards integrating valleytronics, topological quantum effects, and spintronics in a single system. To confirm this aspect, for Fe_2BrMgP with $a/a_0 = 1.04$ at $E = +0.02$ V/Å, the edge states along the [100] direction and the evolution of the Wannier charge centers (WCCs) along k_y are plotted in Fig. 6. Based on the evolution of WCCs, the spin Chern number $|C_s|$ is 2, which is further determined by two pairs of gapless edge states with opposite chiralities appearing in the bulk gap.

It is noteworthy that an out-of-plane electric field can break $\mathcal{PT}$ symmetry by breaking $\mathcal{P}$ symmetry, which can mix the spin-up and spin-down states, and the gaps for edge states will be induced (The AFM QSHI is not well-defined.). However, an out-of-plane electric field 0.02 V/Å is applied in Fe_2BrMgP, and only a very small gap of about 5 meV for edge states is produced. After applying the electric field in Fe_2BrMgP, because the calculated edge states have almost no energy gap, it still maintains relatively good quantum spin characteristics. So, our proposed system Fe_2BrMgP can be approximated as a VQSHI.

IX. CONCLUSION

In summary, we propose a paradigm for achieving the anomalous valley Hall effect in AFM tetragonal monolayers by external field and strain engineering. The proposed concept is confirmed by a prototype monolayer Fe_2BrMgP using first-principles calculations. Uniaxial strain induces valley polarization by breaking C_4 symmetry, and an out-of-plane electric field gives rise to spin splitting via layer-dependent electrostatic potential. The concept of VQSHI is demonstrated, which is similar to VQAHI. Our analysis can be readily extended to the broader family of Fe_2XY ($X =$ or $\neq$ $Y =$ Cl, Br, and I) and Li_2Fe_2XY ($X =$ or $\neq$ $Y =$ S, Se, and Te) bilayers as they share the same Fe-dominated low-energy states as Fe_2BrMgP. The energy band structures for some of these families are shown in Fig. S10 [60], like Fe_2Br_2, Fe_2I_2, Fe_2BrI, $Li_2Fe_2S_2$, $Li_2Fe_2Se_2$, and Li_2Fe_2SSe. Our results reveal a route towards energy-saving and fast-operating spintronic-valleytronic devices based on 2D antiferromagnetic materials.

ACKNOWLEDGMENTS

This work is supported by Natural Science Basis Research Plan in Shaanxi Province of China (Grant No. 2021JM-456). Y.S.A. is supported by the Singapore Ministry of Education Academic Research Fund Tier 2 (Award No. MOE-T2EP50221-0019). We are grateful to Shanxi Supercomputing Center of China, and the calculations were performed on TianHe-2.

[1] J. R. Schaibley, H. Yu, G. Clark, P. Rivera, J. S. Ross, K. L. Seyler, W. Yao, and X. Xu, Valleytronics in 2D materials, Nat. Rev. Mater. **1**, 16055 (2016).

[2] G. Pacchioni, Valleytronics with a twist, Nat. Rev. Mater. **5**, 480 (2020).

[3] S. A. Vitale, D. Nezich, J. O. Varghese, P. Kim, N. Gedik, P. Jarillo-Herrero, D. Xiao, and M. Rothschild, Valleytronics: opportunities, challenges, and paths forward, Small **14**, 1801483 (2018).

[4] D. Xiao, M. C. Chang, and Q. Niu, Berry phase effects on electronic properties, Rev. Mod. Phys. **82**, 1959 (2010).

[5] Y. S. Ang, S. A. Yang, C. Zhang, Z. Ma, and L. K. Ang, Valleytronics in merging Dirac cones: All-electric-controlled valley filter, valve, and universal reversible logic gate, Phys. Rev. B **96**, 245410 (2017).

[6] K. E. J. Goh, C. P. Y. Wong, and T. Wang, *Valleytronics in 2D Materials* (World Scientific, Singapore, 2023).

[7] L. L. Tao, A. Naeemi, and E. Y. Tsymbal, Valley-spin logic gates, Phys. Rev. Appl. **13**, 054043 (2020).

[8] A. Srivastava, M. Sidler, A. V. Allain, D. S. Lembke, A. Kis, and A. Imamoglu, Valley Zeeman effect in elementary optical excitations of monolayer WSe_2, Nat. Phys. **11**, 141 (2015).

[9] K. F. Mak, K. He, J. Shan, and T. F. Heinz, Control of valley polarization in monolayer MoS_2 by optical helicity, Nat. Nanotechnol. **7**, 494 (2012).

[10] H. Zeng, J. Dai, W. Yao, D. Xiao, and X. Cui, Valley polarization in MoS_2 monolayers by optical pumping, Nat. Nanotechnol. **7**, 490 (2012).

[11] M. Zeng, Y. Xiao, J. Liu, K. Yang, and L. Fu, Exploring two-dimensional materials toward the next-generation circuits: from monomer design to assembly control, Chem. Rev. **118**, 6236 (2018).

[12] C. Zhao, T. Norden, P. Zhang, P. Zhao, Y. Cheng, F. Sun, J. P. Parry, P. Taheri, J. Wang, Y. Yang, T. Scrace, K. Kang, S. Yang, G. Miao, R. Sabirianov, G. Kioseoglou, W. Huang, A. Petrou, and H. Zeng, Enhanced valley splitting in monolayer WSe_2 due to magnetic exchange field, Nat. Nanotechnol. **12**, 757 (2017).

[13] D. MacNeill, C. Heikes, K. F. Mak, Z. Anderson, A. Kormányos, V. Zólyomi, J. Park, and D. C. Ralph, Breaking of valley degeneracy by magnetic field in monolayer $MoSe_2$, Phys. Rev. Lett. **114**, 037401 (2015).

[14] W. Y. Tong, S. J. Gong, X. Wan, and C. G. Duan, Concepts of ferrovalley material and anomalous valley Hall effect, Nat. Commun. **7**, 13612 (2016).

[15] J. Zheng, Y. Zhao, Y. Tan, Z. Guan, N. Zhong, F. Yue, P. Xiang, and C. G. Duan, Coupling of ferroelectric and valley properties in 2D materials, J. Appl. Phys. **132**, 120902 (2022).

[16] X. Hu, Half-metallic antiferromagnet as a prospective material for spintronics, Adv. Mater. **24**, 294 (2012).

[17] T. Jungwirth, J. Sinova, A. Manchon, X. Marti, J. Wunderlich, and C. Felser, The multiple directions of antiferromagnetic spintronics, Nat. Phys. **14**, 200 (2018).

[18] W. Du, R. Peng, Z. He, Y. Dai, B. Huang, and Y. Ma, Anomalous valley Hall effect in antiferromagnetic monolayers, npj 2D Mater. Appl. **6**, 11 (2022).

[19] X. Xu, Z. He, Y. Dai, B. Huang, and Y. Ma, Single-valley state in a two-dimensional antiferromagnetic lattice, Phys. Rev. B **104**, 205430 (2021).

[20] W. Zhou, G. Zheng, A. Li, D. Zhang, and F. Ouyang, Orbital contribution to the regulation of the spin-valley coupling in antiferromagnetic monolayer $MnPTe_3$, Phys. Rev. B **107**, 035139 (2023).

[21] X. Li, T. Cao, Q. Niu, J. Shi, and J. Feng, Coupling the valley degree of freedom to antiferromagnetic order, Proc. Natl. Acad. Sci. USA **110**, 3738 (2013).

[22] T. Zhao, S. Xing, J. Zhou, N. Miao, and Z. Sun, Stacking order modulated anomalous valley Hall effect in antiferromagnetic MXene, J. Materiomics **10**, 269 (2024).

[23] C. Nayak, S. H. Simon, A. Stern, M. Freedman, and S. Das Sarma, Non-Abelian anyons and topological quantum computation, Rev. Mod. Phys. **80**, 1083 (2008).

[24] M. Z. Hasan and C. L. Kane, Colloquium: Topological insulators, Rev. Mod. Phys. **82**, 3045 (2010).

[25] X.-L. Qi and S.-C. Zhang, Topological insulators and superconductors, Rev. Mod. Phys. **83**, 1057 (2011).
[26] M. Bora, S. K. Behera, P. Samal, and P. Deb, Magnetic proximity induced valley-contrasting quantum anomalous Hall effect in a graphene-$CrBr_3$ van der Waals heterostructure, Phys. Rev. B **105**, 235422 (2022).
[27] M. Vila, J. H. Garcia, and S. Roche, Valley-polarized quantum anomalous Hall phase in bilayer graphene with layer-dependent proximity effects, Phys. Rev. B **104**, L161113 (2021).
[28] H. Pan, Z. Li, C. C. Liu, G. Zhu, Z. Qiao, and Y. Yao, Valley-polarized quantum anomalous Hall effect in silicene, Phys. Rev. Lett. **112**, 106802 (2014).
[29] J. Zhou, Q. Sun, and P. Jena, Valley-polarized quantum anomalous Hall effect in ferrimagnetic honeycomb lattices, Phys. Rev. Lett. **119**, 046403 (2017).
[30] F. Zhan, Z. Ning, L. Y. Gan, B. Zheng, J. Fan, and R. Wang, Floquet valley-polarized quantum anomalous Hall state in nonmagnetic heterobilayers, Phys. Rev. B **105**, L081115 (2022).
[31] X. D. Zhu, Y. Q. Chen, Z. Liu, Y. L. Han, and Z. H. Qiao, Valley-polarized quantum anomalous Hall effect in van der Waals heterostructures based on monolayer jacutingaite family materials, Front. Phys. **18**, 23302 (2023).
[32] Q. Sui, J. Zhang, S. Jin, Y. Xia, and G. Li, Model Hamiltonian for the quantum anomalous Hall state in iron-halogenide, Chin. Phys. Lett. **37**, 097301 (2020).
[33] Z. Liu, Y. Han, Y. Ren, Q. Niu, and Z. Qiao, Van der Waals heterostructure Pt_2HgSe_3/CrI_3 for topological valleytronics, Phys. Rev. B **104**, L121403 (2021).
[34] S. D. Guo, Y. L. Tao, W. Q. Mu, and B. G. Liu, Correlation-driven threefold topological phase transition in monolayer $OsBr_2$, Front. Phys. **18**, 33304 (2023).
[35] S. Li, Q. Q. Wang, C. M. Zhang, P. Guo, and S. A. Yang, Correlation-driven topological and valley states in monolayer VSi_2P_4, Phys. Rev. B **104**, 085149 (2021).
[36] W. Y. Pan, Tuning the magnetic anisotropy and topological phase with electronic correlation in single-layer H-$FeBr_2$, Phys. Rev. B **106**, 125122 (2022).
[37] S. D. Guo, W.-Q. Mu, J.-H. Wang, Y.-X. Yang, B. Wang, and Y.-S. Ang, Strain effects on the topological and valley properties of the Janus monolayer $VSiGeN_4$, Phys. Rev. B **106**, 064416 (2022).
[38] K. Sheng, B. K. Zhang, H. K. Yuan, and Z. Y. Wang, Strain-engineered topological phase transitions in ferrovalley 2H-$RuCl_2$ monolayer, Phys. Rev. B **105**, 195312 (2022).
[39] P. Liu, S. Liu, M. Jia, H. B. Yin, G. Zhang, F. Ren, B. Wang, and C. Liu, Strain-driven valley states and phase transitions in Janus $VSiGeN_4$ monolayer, Appl. Phys. Lett. **121**, 063103 (2022).
[40] S. D. Guo, G. Wang, and Y. S. Ang, Possible way to achieve valley-polarized quantum anomalous Hall insulator, Appl. Phys. Lett. **123**, 173102 (2023).
[41] Y. H. Zhang, D. Mao, Y. Cao, P. Jarillo-Herrero, and T. Senthil, Nearly flat Chern bands in moiré superlattices, Phys. Rev. B **99**, 075127 (2019).
[42] Y. M. Xie, C. P. Zhang, J. X. Hu, K. F. Mak, and K. T. Law, Valley-polarized quantum anomalous Hall state in moiré $MoTe_2/WSe_2$ heterobilayers, Phys. Rev. Lett. **128**, 026402 (2022).
[43] B. T. Zhou, S. Egan, and M. Franz, Moiré flat Chern bands and correlated quantum anomalous Hall states generated by spin-orbit couplings in twisted homobilayer MoS_2, Phys. Rev. Res. **4**, L012032 (2022).
[44] S. D. Guo and Y. S. Ang, Spontaneous spin splitting in electric potential difference antiferromagnetism, Phys. Rev. B **108**, L180403 (2023).
[45] Q. L. Sun, Y. D. Ma, and N. Kioussis, Two-dimensional Dirac spin-gapless semiconductors with tunable perpendicular magnetic anisotropy and a robust quantum anomalous Hall effect, Mater. Horiz. **7**, 2071 (2020).
[46] Y. Li, J. H. Li, Y. Li, M. Ye, F. W. Zheng, Z. T. Zhang, J. H. Fu, W. H. Duan, and Y. Xu, High-temperature quantum anomalous Hall insulators in lithium-decorated iron-based superconductor materials, Phys. Rev. Lett. **125**, 086401 (2020).
[47] S. D. Guo, W. Q. Mu, X. B. Xiao, and B. G. Liu, Intrinsic room-temperature piezoelectric quantum anomalous Hall insulator in Janus monolayer Fe_2IX (X = Cl and Br), Nanoscale **13**, 12956 (2021).
[48] J. Y. Li, Q. S. Yao, L. Wu, Z. X. Hu, B. Y. Gao, X. G. Wan, and Q. H. Liu, Designing light-element materials with large effective spin-orbit coupling, Nat. Commun. **13**, 919 (2022).
[49] S. D. Guo, Y. T. Zhu, J. L. Xin, and B. G. Liu, Correlation-enhanced spin-orbit coupling in a quantum anomalous Hall insulator Fe_2Br_2 monolayer with a large band gap and robust ferromagnetism, J. Mater. Chem. C **10**, 8381 (2022).
[50] S. D. Guo, W. Q. Mu, M. Y. Yin, Y. C. Li, and W. C. Ren, Coexistence of intrinsic piezoelectricity, ferromagnetism, and nontrivial band topology in Li-decorated Janus monolayer Fe_2SSe with a high Curie temperature, J. Phys. D: Appl. Phys. **54**, 505006 (2021).
[51] Y. Xue, W. Xu, B. Zhao, J. Zhang, and Z. Yang, Antiferromagnetic quantum spin Hall insulators with high spin Chern numbers, Phys. Rev. B **108**, 075138 (2023).
[52] P. Hohenberg and W. Kohn, Inhomogeneous electron gas, Phys. Rev. **136**, B864 (1964); W. Kohn and L. J. Sham, Self-consistent equations including exchange and correlation effects, *ibid.* **140**, A1133 (1965).
[53] G. Kresse, *Ab initio* molecular dynamics for liquid metals, J. Non-Cryst. Solids **192-193**, 222 (1995).
[54] G. Kresse and J. Furthmüller, Efficiency of *ab-initio* total energy calculations for metals and semiconductors using a plane-wave basis set, Comput. Mater. Sci. **6**, 15 (1996).
[55] G. Kresse and D. Joubert, From ultrasoft pseudopotentials to the projector augmented-wave method, Phys. Rev. B **59**, 1758 (1999).
[56] J. P. Perdew, K. Burke, and M. Ernzerhof, Generalized gradient approximation made simple, Phys. Rev. Lett. **77**, 3865 (1996).
[57] S. L. Dudarev, G. A. Botton, S. Y. Savrasov, C. J. Humphreys, and A. P. Sutton, Electron-energy-loss spectra and the structural stability of nickel oxide: An LSDA+U study, Phys. Rev. B **57**, 1505 (1998).
[58] A. A. Mostofia, J. R. Yatesb, G. Pizzif, Y.-S. Lee, I. Souzad, D. Vanderbilte, and N. Marzarif, An updated version of wannier90: A tool for obtaining maximally-localised Wannier functions, Comput. Phys. Commun. **185**, 2309 (2014).
[59] Q. Wu, S. Zhang, H. F. Song, M. Troyer, and A. A. Soluyanov, WannierTools: An open-source software package for novel

topological materials, Comput. Phys. Commun. **224**, 405 (2018).

[60] See Supplemental Material at http://link.aps.org/supplemental/10.1103/PhysRevB.109.134426 for the magnetic configurations; the related energy band structures; the energy differences between FM/AFM2/AFM3 and AFM1 orderings; MAE; and Berry curvature distribution.

[61] K. N. Duerloo, M. T. Ong, and E. J. Reed, Intrinsic piezoelectricity in two-dimensional materials, J. Phys. Chem. Lett. **3**, 2871 (2012).

[62] C. Lee, X. Wei, J. W. Kysar, and J. Hone, Measurement of the elastic properties and intrinsic strength of monolayer graphene, Science **321**, 385 (2008).

[63] X. Zhou, R.-W. Zhang, Z. Zhang, W. Feng, Y. Mokrousov, and Y. Yao, Sign-reversible valley-dependent Berry phase effects in 2D valley-half-semiconductors, npj Comput. Mater. **7**, 160 (2021).

[64] C. L. Kane and E. J. Mele, Quantum spin Hall effect in graphene, Phys. Rev. Lett. **95**, 226801 (2005).